# Importance of orographic gravity waves over the Tibetan plateau on the spring rainfall in East Asia

Article

Accepted Version

It is advisable to refer to the publisher's version if you intend to cite from the work.  See Guidance on citing.

www.reading.ac.uk/centaur

# CentAUR

Central Archive at the University of Reading

Reading's research outputs online

# Importance of orographic gravity waves over the Tibetan Plateau on the spring rainfall in East Asia

Runqiu LI[1], Xin XU[1*], Xiangde XU[2†], Theodore G. SHEPHERD[3], & Yuan WANG[1]


[1]*Key Laboratory of Mesoscale Severe Weather/Ministry of Education and School of Atmospheric Sciences, Nanjing University, Nanjing 210023, China;*

[2]*State Key Laboratory of Severe Weather, Chinese Academy of Meteorological Sciences, Beijing 100081, China;*

[3]*Department of Meteorology, University of Reading, Earley Gate, PO Box 243, Reading RG6 6BB, UK*

\* *Corresponding author (email: xinxu@nju.edu.cn)*

† *Corresponding author (email: xuxd@cma.gov.cn)*

## Abstract

The springtime persistent rainfall (SPR) is the major rainy period before the onset of summer monsoon in East Asia, which profoundly affects the regional and even global hydrological cycle. Despite the great importance of the mechanical and thermal effects of the Tibetan Plateau (TP) large-scale orography on the formation of SPR, the impact of small-scale orography over the TP remains poorly understood. Here we show that upward-propagating orographic gravity waves (OGWs), which occur as the subtropical westerlies interact with the TP's small-scale orography, contribute importantly to the SPR. The breaking of OGWs induces a large zonal wave drag in the middle troposphere, which drives a meridional circulation across the TP. The rising branch of the meridional circulation acts to lower the pressure and increase the meridional pressure gradient to the south of the TP by dynamically pumping the lower-tropospheric air upwards. The southwesterly monsoonal flow on the southeastern flank of the TP thus intensifies and transports more water vapor to East Asia, resulting in an enhancement of the SPR. This finding helps more completely understand the impacts of TP's multiscale orography on the SPR and provides a new perspective on the westerly-monsoon synergy in East Asia.

## 1. Introduction

In boreal spring (i.e., March to May), persistent rainfall often occurs in East Asia, forming a rain belt that stretches from South China to the east of Japan. This springtime persistent rainfall (SPR) accounts for about 35% of the annual precipitation in South China, which brings plentiful water for agricultural and industrial use but can also cause heavy rainfall and flash flooding (Ding, 2019; Luo et al., 2017; Li et al., 2018). Moreover, large amounts of stratus clouds are generated in East Asia during SPR, which play a vital role in the regional and even global energy budget and hydrological cycle via the cloud radiative effect (e.g., Wang et al., 2014; Li et al., 2019).

The formation of SPR in East Asia is closely related to the water vapor transport by the southwesterly monsoonal flow originating from the Indian Ocean (Zhao et al., 2007). Tian and Yasunari (1998) attributed the southwesterlies to the west-east thermal contrast between the Indochina Peninsula and the western North Pacific, owing to the time-lag of seasonal warming in spring. However, Wan and Wu (2007) concluded that the southwesterlies are climatically caused by the mechanical and thermal forcings of the Tibetan Plateau (TP) using numerical sensitivity experiments. For one thing, the mid-latitude westerly flow is blocked by the large-scale orography of the TP and splits into northern and southern branches that reconverge downstream of the plateau (Yeh, 1950). The southwesterly flow is just part of the southern branch of the mechanically-deflected flow. For another, the sensible heating (SH) at the surface of the TP can induce a low-level cyclonic circulation through the sensible heating air pump (SHAP) effect (Wu et al., 2007), which additionally strengthens the southwesterly flow (Wu et al., 2012). Although the mechanical and thermal effects of the TP's large-scale orography are generally well represented in climate models, the SPR and stratus clouds in East Asia are systematically underestimated in even *state-of-the-art* climate models, e.g., models adopted by Phase 6 of the Coupled Model Intercomparison Project (CMIP6) and the modern-era reanalysis datasets (Li et al., 2018; Wang et al., 2014) (see Figure S1).

Given its complex terrain, the TP consists of multiscale orography, including not only the large-scale plateau but also small-scale mountains of horizontal lengths ranging from a few to tens of kilometers that cannot be fully resolved in climate models, i.e., subgrid-scale

orography (SSO). These small-scale mountains are capable of triggering upward-propagating orographic gravity waves (OGWs) which can produce a drag force known as orographic gravity wave drag (OGWD) via wave breaking. It has been well recognized that OGWD can notably affect the atmospheric circulation at both global and regional scales, such as the Brewer-Dobson circulation in the middle atmosphere and the tropospheric jets, blocking and storm tracks (e.g., Sigmond and Shepherd, 2014; Pithan et al., 2016; Choi et al., 2017; Sato and Hirano, 2019; Zhang et al., 2020). The TP is one of the OGW hotspots around the world which provides the largest source of OGWD (Eckermann and Preusse, 1999; Sato et al., 2009). Recently, there is a growing interest in the impacts of OGWD over the TP. For instance, Šácha et al. (2021) revealed that the strong OGWD over the TP can decelerate the polar vortex by enhancing the upward propagation of planetary Rossby waves into the polar stratosphere. Cohen and Boos (2016) found a close relation between the Madden-Julian oscillation (MJO) convective activities and the TP's OGWD in winter. The incoporation of OGWD parameterization in numerical models can improve the simulations of wintertime circulation and precipitation over the TP (Zhou et al., 2017). However, the impacts of OGWD over the TP on the springtime rainfall in East Asia has rarely been considered.

Here, we found that SPR is substantially weaker in the absence of OGWD, indicating the previously unreported importance of small-scale orography over the TP. The OGWD can dynamically drive a meridional circulation across the TP, which acts like an air pump in a similar manner to the well-known SHAP induced by the large-scale orography of the TP. This dynamical air pump can notably strengthen the low-level southwesterly flow on the southeastern flank of the TP and hence enhance SPR in East Asia.

## 2. Materials and methods

### 2.1 Precipitation and reanalysis datasets

The Climate Prediction Center Morphing (CMORPH) precipitation (Joyce et al., 2004) during 2000–2017 is utilized, with a temporal resolution of 3 hours and horizontal grid spacing of 0.25°. Also used are the simulated precipitation in 12 high-resolution CMIP6 models (see Table. S1). For the atmospheric conditions, the 6-hourly, 0.75° ERA-Interim reanalysis (Dee et al., 2011) is used, which is produced by the Integrated Forecasting System

(IFS) at the European Centre for Medium-Range Weather Forecasts (ECMWF). Moreover, the ERA-Interim reanalysis provides the initial and boundary conditions for the ARW Weather Research and Forecast (WRF) simulations described below.
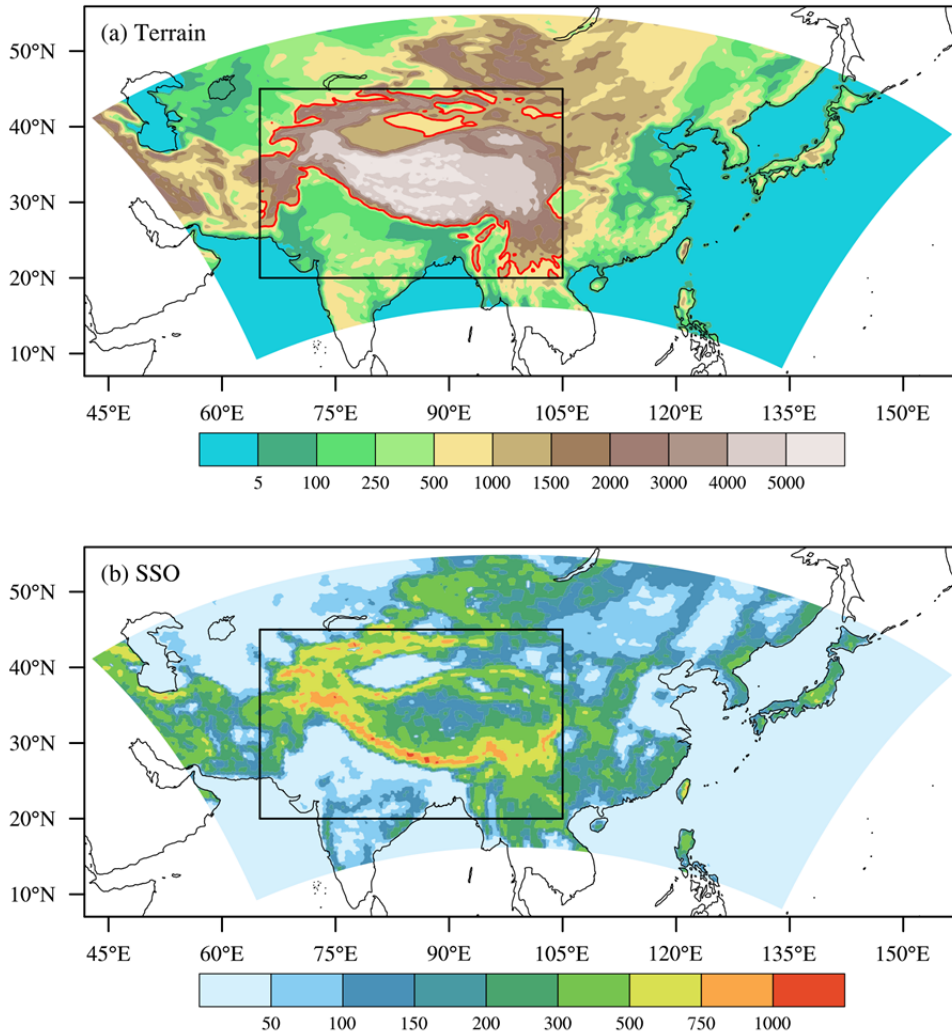


**Figure 1** (a) Terrain elevation (unit: m) and (b) standard deviation of subgrid-scale orography (unit: m) in the WRF model. Red contours in (a) represent the terrain elevation of 1 km. Black rectangles represent the region of the TP (20–45°N, 65–105°E).

## 2.2 Model configuration and design of numerical experiments

The springtime rainfall in East Asia during 2000–2017 is simulated using the WRF-ARW (V4.0), with a horizontal resolution of 27 km (Figure 1a). The model is configured with 50 vertical levels, with the model top located at 30 hPa. For the model physics, the WRF single-

moment 5-class scheme (WSM5) is employed for microphysics, along with the Kain–Fritsch convective scheme, the Yonsei University (YSU) planetary boundary layer scheme, the Noah land surface model, and the Community Atmosphere Model (CAM) for both longwave and shortwave radiation. The effect of OGWD is parameterized using the scheme developed by Kim and Doyle (2005).

Three sets of numerical experiments are conducted. In the control simulation (CTL) the parameterization of OGWD is activated over the whole domain. In the TP_NoOGWD experiment, we turn off the OGWD in the TP area (black box in Figure 1b) by removing the SSO there. (This is achieved by setting the standard deviation of SSO to zero, which has no influence on the model resolved orography.) The difference between the two experiments (CTL minus TP_NoOGWD) therefore reflects the impacts of the parameterized OGWD over the TP. As noted in introduction, previous studies found an important role of surface SH over the TP on the springtime rainfall in East Asia. To examine the relative importance of OGWD and SH, we perform another sensitivity experiment, i.e., TP_NoSH in which surface SH is turned off in the TP region (>1 km terrain elevation, i.e., red isoline in black box in Figure 1a) by setting the variable SHEAT (which denotes sensible heat flux) to zero in the Noah LSM parameterization scheme. All three numerical experiments consist of 18 individual runs, each of which starts on 0000 UTC of 15 February and ends on 0000 UTC of 1 June in each year of 2000–2017.


## 3. Simulated rainfall and circulation in East Asia

Figures 2a–d display the spatial distributions of the observed and simulated spring rainfall in East Asia during 2000–2017. In the CTL experiment, the WRF model well captures the southwest-northeast orientated rain belt in East Asia which stretches from South China to the east of Japan (Figure 2b). Although the intensity of the rainfall center in southeastern China (SEC) is a little bit stronger than observations, both its interannual variability and intraseasonal evolution revealed in Figures 2e, f are successfully reproduced. The correlation coefficients between the time series of the observed and simulated rainfall exceed 0.9 which is statistically significant at the 99% confidence level according to the student-$t$ test.

When the parameterized OGWD is turned off in the TP region, the WRF model still

captures the elongated rain belt in East Asia (Figure 2c) and its temporal variation (Figures 2e, f). Nevertheless, the rainfall intensity is notably underestimated, especially in SEC. There is a remarkable decrease in rainfall in the TP_NoSH experiment as well (Figure 2d) which is as expected given the role of SHAP (Wu et al., 2007). Taking the rainfall center in SEC as an example, the mean rainfall intensity (averaged within the black box in Figure 2a) is underestimated by ~24% and 34% in the TP_NoOGWD and TP_NoSH, respectively. A close examination of their daily evolution reveals that the simulated rainfall in TP_NoOGWD has an intensity nearly the same as that in TP_NoSH during early and middle spring, while the latter shows a larger underestimation in May (Figure 2f). This is owing to that the OGWD over the TP generally decreases from winter to summer (Xu et al., 2017), in contrast to the increasing strength of surface SH during this period (Chen et al., 2019).
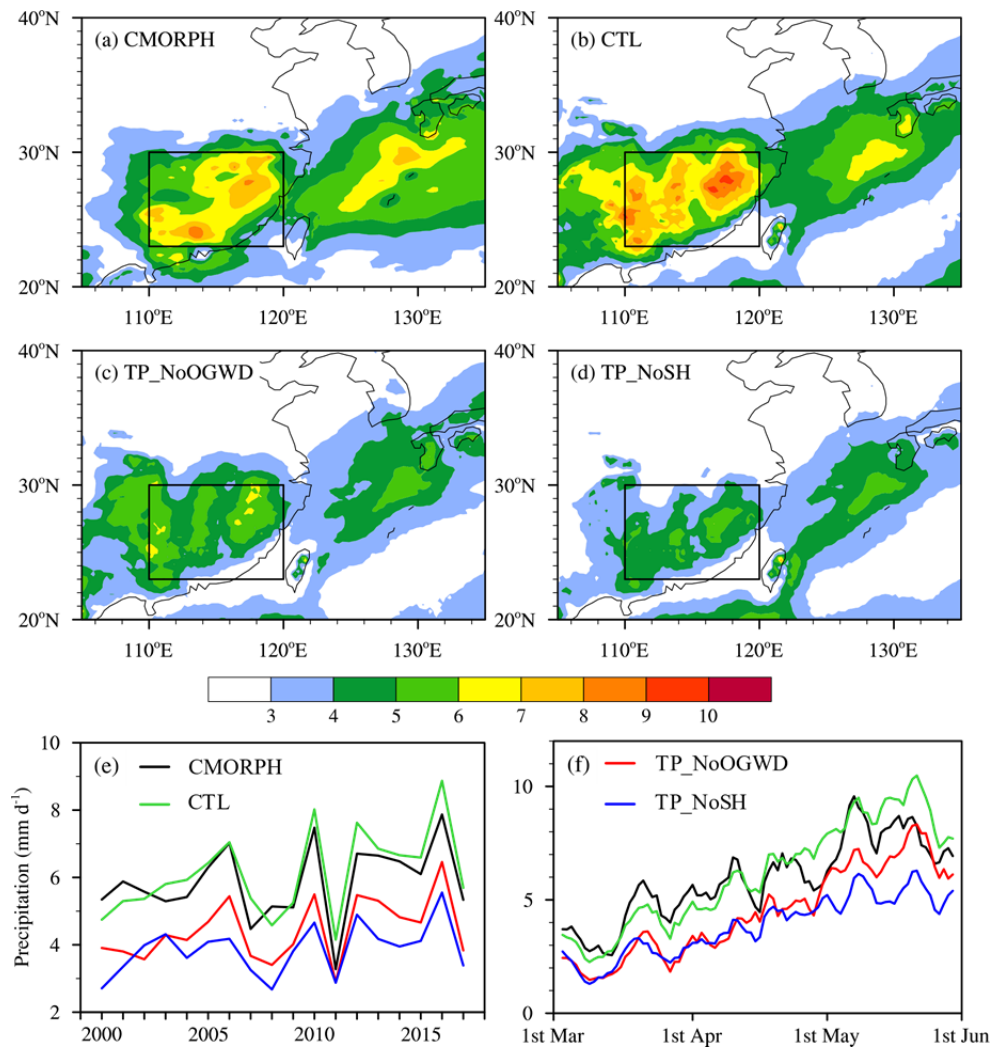


**Figure 2** Spatial distribution of spring rainfall (unit: mm d$^{-1}$) in East Asia obtained from (a)

CMORPH and (b) CTL, (c) TP_NoOGWD and (d) TP_NoSH experiments during 2000–2017. (e) Interannual variability and (f) intraseasonal evolution of spring rainfall (unit: mm d$^{-1}$) in southeastern China (see black rectangles in (a–d)) during 2000–2017. A 5-point running average is applied in (f).

From the above analyses, the OGWD over the TP has a dramatical impact on the SPR in East Asia which is at least comparable to that of surface SH of the TP's large-scale orography. The impact of OGWD is proved to be robust by additional sensitivity experiments configured with different model physics (cumulus convection, radiation, etc.; see Figure S2). In line with the weakened rainfall in East Asia, the shortwave cloud radiation (SWCR) at the top of the atmosphere (TOA) also decreases in the TP_NoOGWD experiment (Figure S3). This agrees with Li et al. (2015) and Zhang et al. (2014) in that the simulated springtime rainfall and stratus clouds in East Asia are increased with finer model horizontal resolution because more scales of orography are resolved by the model.

Previous studies revealed that the water vapor transport by low-level southwesterly monsoonal flow to the south of the TP is crucial for the onset and maintenance of SPR in East Asia (e.g., Zhao et al., 2007; Tian and Yasunari, 1998). Figures 3a–d present the wind circulation and water vapor transport at 850 hPa. The CTL simulation captures the southwesterly winds detouring around the TP and the water vapor transport from the Bay of Bengal (BOB) to East Asia (Figures 3a, b). In the two experiments of TP_NoOGWD and TP_NoSH (Figures 3c, d), the low-level flow south of the TP becomes much weaker than in CTL (Figures 3e, f), which thus can no longer climb over the mountains in the Indochina Peninsula. Instead, it is deflected northward or northwestward toward the TP, resulting in a notable reduction of water vapor transport from the BOB (Figures 3c, d). Furthermore, in response to the weakened southwesterly flow, the western Pacific subtropical high (WPSH) extends more westward, which acts to suppress the upward motion in South China and contributes to the decrease of SPR as well.

Indeed, the CTL simulation produces stronger westerly and southwesterly winds than TP_NoOGWD and TP_NoSH in a broad area from about 60°E to 140°E between 20°N and 30°N. In the case of the difference with TP_NoSH (Figure 3f), a plateau-scale cyclonic

7

circulation is found over the TP and surrounding areas, accompanied by negative perturbations of geopotential height (GPH). This is in agreement with the large-scale air pumping driven by the surface SH over the TP, i.e., the SHAP effect (Wu et al., 2007). The westerly flow is accelerated on the southern flank of the TP where the meridional pressure gradient is enhanced. For the difference with TP_NoOGWD (Figure 3e), negative GPH perturbations are generally confined to the south of the TP, with predominantly positive GPH perturbations to the north/northeast of the TP. This circulation pattern is qualitatively similar to the asymmetric dipole in winter which is due to the mechanical deflection of the impinging subtropical westerlies by the TP's large-scale orography (Wu et al., 2015). As will be shown in section 4 below, the dipole pattern in Figure 3e is caused by the OGWD over the TP which dynamically drive a meridional circulation across the plateau. Note that the SHAP effect has little contribution to the cyclonic circulation difference to the south of the TP between CTL and TP_NoOGWD. There is spatially inhomogeneous variation of SH over the TP (Figure S4c). The weakening of western surface SH is likely owing to the deceleration of near-surface wind by the OGWD.
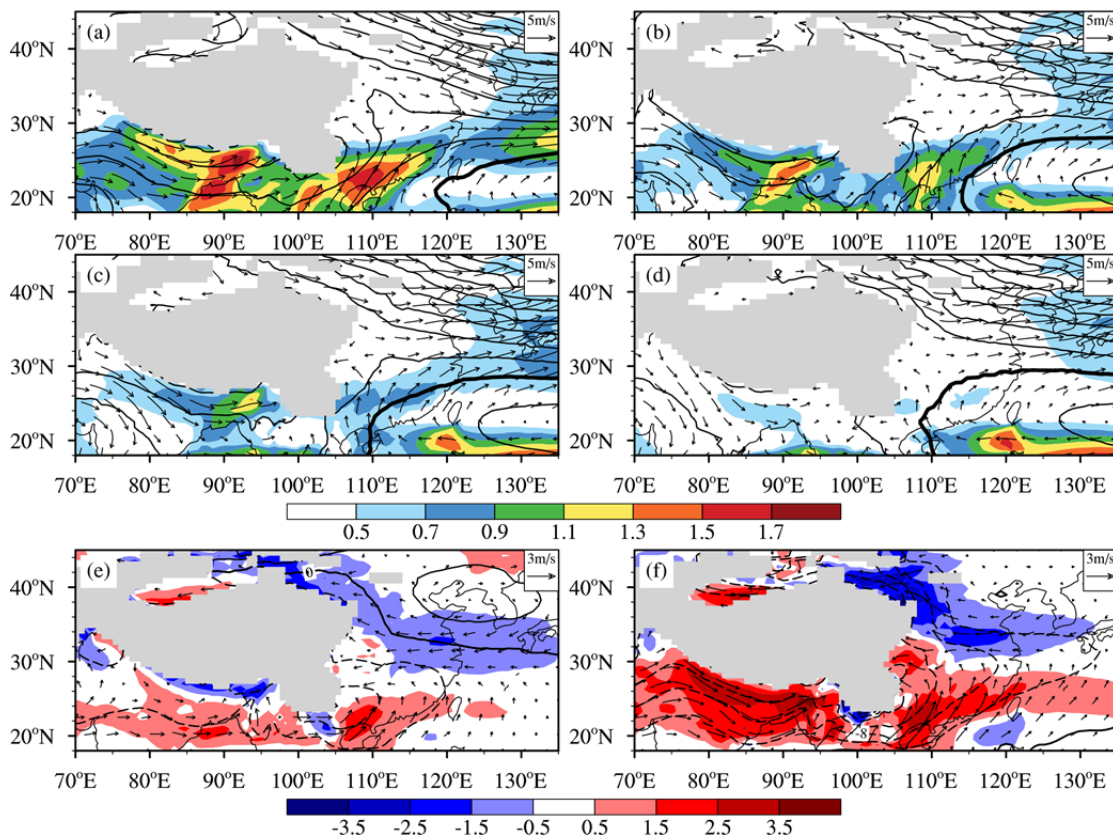
**Figure 3** (a–d) Geopotential height (contours; unit: gpm, at an interval of 10 gpm) and horizontal wind (vectors) at 850 hPa obtained from (a) ERA-Interim and the (b) CTL, (c) TP_NoOGWD and (d) TP_NoSH experiments in spring of 2000–2017. Color shading is for the magnitude of water vapor flux integrated from 1000 to 700 hPa (unit: kg m$^{-1}$ s$^{-1}$). Thick black lines denote the geopotential height of 1510 gpm which marks the bounday of the western Pacific subtropical high. (e–f) are the differences between (b) and (c–d), respectively, but with color shading for the magnitude of horizonal wind speed (unit: m s$^{-1}$).

## 4. Dynamical impacts of OGWD over the TP

Figure 4a shows the distribution of OGWD at 500 hPa in the CTL experiment. Remarkable OGWD are found in western, central and southeastern TP which are mainly westward. Moreover, the OGWD regions are concentrated in the middle troposphere, with little drag in the lower levels. As a result, the 500-hPa westerlies over the TP are directly decelerated by the elevated OGWD (Figure 4b). Based on the quasi-geostrophic approximation to the zonal momentum equation taking into account the OGWD, i.e.,

$$\frac{du}{dt} - fv = -\frac{1}{\rho}\frac{\partial p}{\partial x} + OGWD_x, \tag{1}$$

which, for steady large-scale flow with little downstream variation, can be simplified to

$$-fv_a = OGWD_x \ , \tag{2}$$

the deceleration of westerly flow by zonal drag will induce an ageostrophic southerly flow ($v_a$). Figure 4c clearly shows southerly wind components above the plateau. This poleward-moving airflow produces an eastward Coriolis torque that acts to balance the westward OGWD. Under the constraint of mass continuity in the meridional plane, i.e., $\frac{\partial v}{\partial y} + \frac{\partial w}{\partial p} = 0$, upward and downward motions are induced to the south and north of the plateau, respectively, forming a meridional circulation across the TP (Figure 4c). Physically, the poleward movement of ageostrophic southerly flow causes a mid-tropospheric pressure minimum on the southern side of the TP, leading to an upward pressure gradient force which dynamically pumps the lower-tropospheric air upwards and thus maintains the meridional circulation (Haynes and Shepherd, 1989). The pressure deficit in the lower troposphere tends to increase the meridional pressure gradient and strengthen the low-level

9

westerly/southwesterly winds to the south of the TP (Figure 3e). This acceleration can be viewed as an indirect response of the model resolved dynamics to parametrized OGWD, consistent with van Niekerk et al. (2018) (see their Figures 3b, 8b).
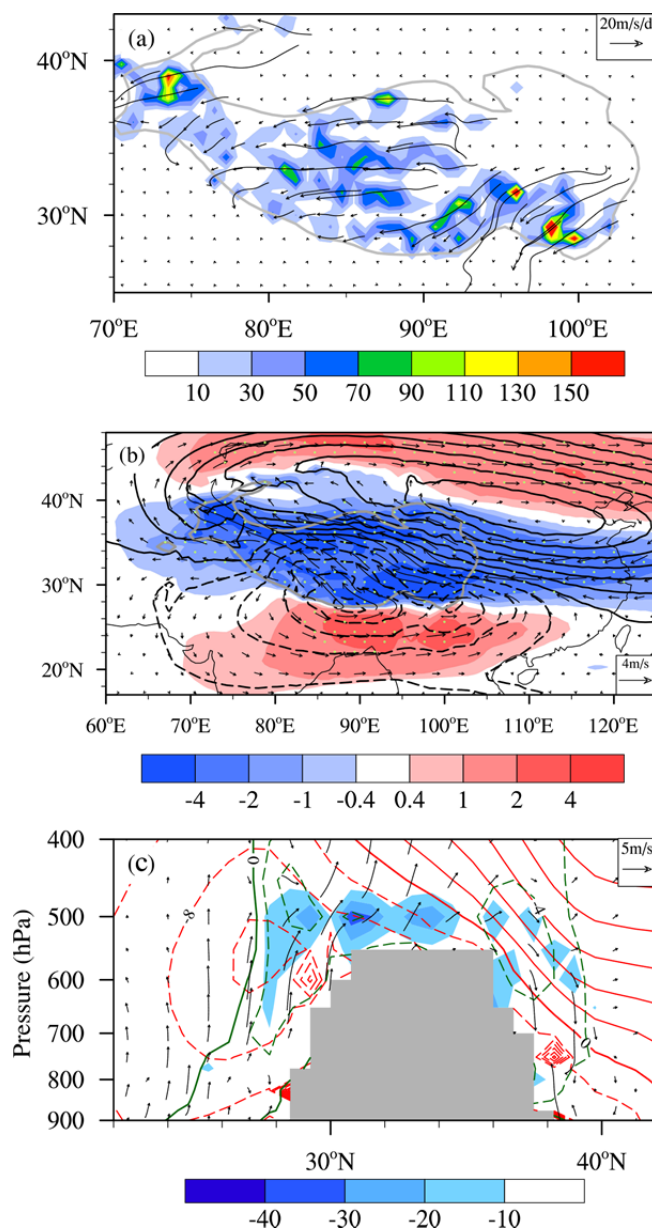


**Figure 4** (a) Zonal and meridional OGWD vector and its magnitude (shading; unit: m s$^{-1}$ d$^{-1}$) at 500 hPa in spring of 2000–2017 obtained from the CTL experiment. (b) Differences between the 500-hPa geopotential heights (black contours; unit: gpm, at an interval of 5 gpm) and horizontal winds (vectors) and speeds (shading; unit: m s$^{-1}$) in CTL and TP_NoOGWD (i.e. CTL minus TP_NoOGWD). White stippling indicates horizontal speed difference that is statistically significant at 95% confidence level using the student-*t* test. (c) Differences

10

between the zonal-mean geopotential heights (red contours; unit: gpm, at an interval of 4 gpm) and zonal winds (dark green contours; unit: m s$^{-1}$, at an interval of 2 m s$^{-1}$) in CTL and TP_NoOGWD averaged between 85°E to 95°E. Vectors denote the differences of wind in the meridional plane with the vertical velocity enlarged by 100 times for clarity, while shading indicates the zonal-mean zonal OGWD (unit: m s$^{-1}$ d$^{-1}$) in CTL. Grey contours in (a) and (b) are the 3000-m elevation.

This cross-plateau meridional circulation is qualitatively similar to the secondary circulation induced by an upper-level westward wave forcing, which can be quantified according to the "downward-control" theory (Haynes et al., 1991). To better reveal the impact of OGWD over the TP, this theory is employed herein to diagnose the vertical velocity in response to the OGWD. Although it was originally derived for the response to zonally symmetric wave forcing, the "downward-control" theory is also applicable to zonally asymmetric wave forcing (Shaw and Boos, 2012).

In the situation of steady zonal wave forcing ($\bar{G}$), the vertical velocity associated with the secondary circulation is given by

$$\omega(p) = \frac{\partial}{r \partial \varphi}\left[\frac{1}{f}\int_p^0 \bar{G}\, dp\right], \tag{3}$$

where $\omega$ is the vertical velocity in isobaric coordinates, $r$ is the earth's radius, and $\varphi$ is the latitude. At a given level, the wave-induced vertical velocity is proportional to the meridional gradient of vertically-integrated wave forcing above this level. Figure 5a shows the distribution of vertically-integrated zonal OGWD from above 500 hPa as an example, which is averaged between 85–95°E where the meridional circulation is most remarkable. The integrated OGWD peaks at about 31°N, giving rise to a negative (positive) meridional gradient of OGWD and thus ascent (descent) motion to the south (north) of the TP. The vertical velocity diagnosed from the "downward-control" theory ($\omega_D$) is compared to its model counterpart, i.e., the difference in vertical velocity ($\omega_d$) between CTL and TP_NoOGWD. Generally, $\omega_D$ shows good agreement with $\omega_d$, in particular for the rising branch of the meridional circulation (Figures 5b, c). This thus helps demonstrate the importance of OGWD over the TP in driving the meridional circulation across the plateau.
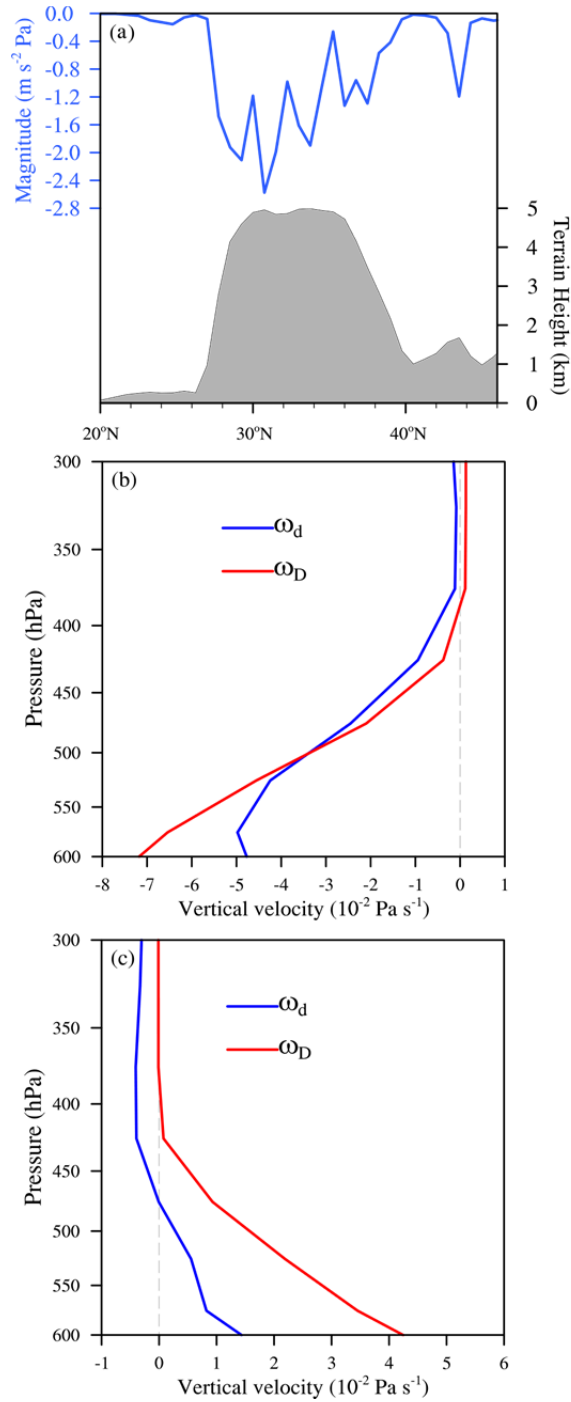
**Figure 5** (a) Meridional distribution of vertically-integrated zonal OGWD above 500 hPa (unit: m s$^{-2}$ Pa) averaged between 85–95°E in spring of 2000–2017 obtained from the CTL experiment. Grey shading represents the corresponding zonal-mean terrain (unit: km). Profiles of $\omega_D$ (vertical velocity diagnosed from the downward-control theory; red line) and $\omega_d$ (difference in vertical velocity between CTL and TP_NoOGWD; blue line) averaged in the (b) rising (23–27°N; 85–95°E) and (c) sinking (37–41°N; 85–95°E) branches of the OGWD-driven meridional circulation across the TP.

## 5. Discussions

In this study, we found that the OGWs triggered by small-scale orography over the TP contribute importantly to the spring rainfall in East Asia. A new type of air pump is proposed, which is in analogy to the well-known thermal air pump (i.e., SHAP) but driven by the OGWD. The mid-tropospheric OGWD perturbs the geostrophic balance of the large-scale westerly flow over the TP and drives a meridional circulation across the TP (Figure 6). To the south of the TP, the rising branch of the meridional circulation dynamically pumps the lower-tropospheric air upwards, creating a pressure depression that acts to increase the meridional pressure gradient. In consequence, the southwesterly monsoonal flow on the southeastern flank of the TP is strengthened, favoring the water vapor transport from the BOB to East Asia. Without the OGWD over the TP, the SPR is much weaker.
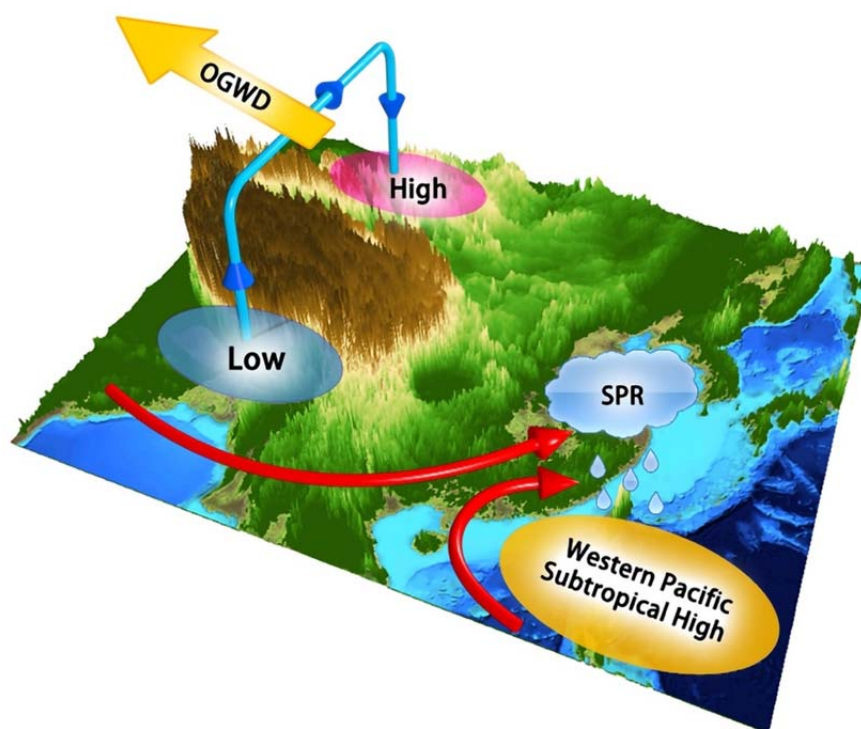


**Figure 6** Conceptual model for the dynamical impacts of OGWD over the TP on the SPR in East Asia.

The impact of OGWD over the TP on the SPR is comparable to that of surface SH of the TP's large-scale orography, both of which can notably influence the wind circulation and water vapor transport in the TP and the sourrounding area. Unlike the SHAP effect, the OGWD occurs as westerlies perturbed by the small-scale complex terrain, which is thus most prominent in the cold season (from winter to mid-spring) (Li et al., 2020). By contrast, the surface SH over the TP peaks in late spring and summer (Fu et al., 2020). The OGWD-induced dynamical air pump manifests as an important, but unreported, pathway of westerly-monsoon synergy (Xu et al., 2014; Chen et al., 2021) in affecting the rainfall and hydrological cycle in the East Asian monsoon region.

The finding also has important implications for the simulation and future projection of SPR in climate models. It is critical to accurately represent the dynamical and thermal effects of TP's multiscale orography in climate models. Under a warming climate, future changes of regional rainfall are of both scientific and societal interest. The SPR has been reported to experience a decreasing trend in recent decades which threatens the water resources for agricultural and industrial use (Li et al., 2018; Zhang et al., 2020). Large uncertainties exist in the projections of regional rainfall changes, however. The OGWD is notoriously difficult to represent and remains one of the major sources of uncertainty in climate change projections (Shepherd, 2014; Sandu et al., 2019). New knowledge of gravity wave dynamics (e.g., Kruse, 2020; Xu et al., 2021; Teixeira and Argain, 2022; Zhou et al., 2019) as well as new technologies like deep learning to emulate and/or optimize gravity wave parameterizations (e.g., Matsuoka et al., 2020; Espinosa et al., 2022) are required to achieve a better representation of small-scale orographic effects in the regions of complex terrain such as the TP.

**References**

Chen F, Ding L, Piao S, Zhou T, Xu B, Yao T, Li X. 2021. The Tibetan Plateau as the engine

for Asian environmental change: the Tibetan Plateau Earth system research into a new era. Sci Bull, 66: 1263–1266

Chen L, Pryor S C, Wang H, Zhang R. 2019. Distribution and variation of the surface sensible heat flux over the central and eastern Tibetan Plateau: Comparison of station observations and multireanalysis products. J Geophys Res, 124: 6191–6206

Choi H J, Choi S J, Koo M S, Kim J E, Kwon Y C, Hong S Y. 2017. Effects of parameterized orographic drag on weather forecasting and simulated climatology over East Asia during boreal summer. J Geophys Res, 122: 10669–10678

Cohen N Y, Boos W R. 2016. Modulation of subtropical stratospheric gravity waves by equatorial rainfall. Geophys Res Lett, 43: 466–471

Ding Y. 2019. The major advances and development process of the theory of heavy rainfalls in China. Torr Rain Dis, 38: 395–406 (in Chinese)

Dee D P, Uppala S M, Simmons A J, Berrisford P, Poli P, Kobayashi S, Andrae U, Balmaseda M A, Balsamo G, Bauer P, Bechtold P, Beljaars A C M, van de Berg L, Bidlot J, Bormann N, Delsol C, Dragani R, Fuentes M, Geer A J, Haimberger L, Healy S B, Hersbach H, Hólm E V, Isaksen L, Kållberg P, Köhler M, Matricardi M, McNally A P, Monge-Sanz B M, Morcrette J J, Park B K, Peubey C, de Rosnay P, Tavolato C, Thépaut J N, Vitart F. 2011. The ERA-Interim reanalysis: configuration and performance of the data assimilation system. Q J R Meteorol Soc, 137: 553–597

Eckermann S D, Preusse P. 1999. Global measurements of stratospheric mountain waves from space. Science, 286: 1534–1537

Espinosa Z I, Sheshadri A, Cain G R, Gerber E P, DallaSanta K J. 2022. Machine learning gravity wave parameterization generalizes to capture the QBO and response to increased $CO_2$. Geophys Res Lett, 49: e2022GL098174

Fu Y, Ma Y, Zhong L, Yang Y, Guo X, Wang C, Xu X, Yang K, Xu X, Liu L, Fan G, Li Y, Wang D. 2020. Land-surface processes and summer-cloud-precipitation characteristics in the Tibetan Plateau and their effects on downstream weather: a review and perspective. Nat Sci Rev, 7: 500–515

Haynes P H, Marks C J, Mcintyre M E, Shepherd T G, Shine K P. 1991. On the "downward control" of extratropical diabatic circulations by eddy-induced mean zonal forces. J Atmos

Sci, 48: 651–678

Haynes P H, Shepherd T G. 1989. The importance of surface pressure changes in the response of the atmosphere to zonally-symmetric thermal and mechanical forcing. Q J R Meteorol Soc, 115: 1181–1208

Joyce R J, Janowiak J E, Arkin P A, Xie P. 2004. CMORPH: A method that produces global precipitation estimates from passive microwave and infrared data at high spatial and temporal resolution. J Hydrometeorol, 5: 487–503

Kim Y J, Doyle J D. 2005. Extension of an orographic-drag parametrization scheme to incorporate orographic anisotropy and flow blocking, Q J R Meteorol Soc, 131: 1893–1921

Kruse C G. 2020. Regional to global evolution of impacts of parameterized mountain-wave drag in the lower stratosphere. J Clim, 33: 3093–3106

Li J, Wang W, Mao J, Wang Z, Zeng G, Chen G. 2019. Persistent spring shortwave cloud radiative effect and the associated circulations over southeastern China. J Clim, 32: 3069–3087

Li J, Yu R, Yuan W, Chen H, Sun W, Zhang Y. 2015. Precipitation over East Asia simulated by NCAR CAM5 at different horizontal resolutions. J Adv Model Earth Syst, 7: 774–790

Li P, Zhou T, Chen X. 2018. Water vapor transport for spring persistent rains over southeastern China based on five reanalysis datasets. Clim Dyn, 51: 4243–4257

Li R, Xu X, Wang Y, Teixeira M A C, Tang J, Lu Y. 2020. The Response of Parameterized Orographic Gravity Waves to Rapid Warming over the Tibetan Plateau. Atmosphere, 11: 1016

Luo Y, Zhang R, Wan Q, Wang B, Wong W K, Hu Z, Jou B J D, Lin Y, Johnson R H, Chang C P, Zhu Y, Zhang X, Wang H, Xia R, Ma J, Zhang D L, Gao M, Zhang Y, Liu X, Chen Y, Huang H, Bao X, Ruan Z, Cui Z, Meng Z, Sun J, Wu M, Wang H, Peng X, Qian W, Zhao K, Xiao Y. 2017. The Southern China Monsoon Rainfall Experiment (SCMREX). Bull Am Meteorol Soc, 98: 999–1013

Matsuoka D, Watanabe S, Sato K, Kawazoe S, Yu, W, Easterbrook, S. 2020. Application of deep learning to estimate atmospheric gravity wave parameters in reanalysis data sets. Geophys Res Lett, 47: e2020GL089436

Pithan F, Shepherd T G, Zappa G, Sandu I. 2016. Climate model biases in jet streams, blocking and storm tracks resulting from missing orographic drag. Geophys Res Lett, 43: 7231–7240

Sacha P, Kuchar A, Eichinger R, Pisoft P, Jacobi C, Rieder H E. 2021. Diverse dynamical response to orographic gravity wave drag hotspots—a zonal mean perspective. Geophys Res Lett, 48: e2021GL093305

Sandu I, van Niekerk A, Shepherd T G, Vosper S B, Zadra A, Bacmeister J, Beljaars A, Brown A R, Dornbrack A, McFarlane N, Pithan F, Svensson G. 2019. Impacts of orography on large-scale atmospheric circulation. Npj Clim Atmos Sci, 2

Sato K, Hirano S. 2019. The climatology of the Brewer-Dobson circulation and the contribution of gravity waves. Atmos Chem Phys, 19: 4517–4539

Sato K, Watanabe S, Kawatani Y, Tomikawa Y, Miyazaki K, Takahashi M. 2009. On the origins of mesospheric gravity waves. Geophys Res Lett, 36: L19801

Shaw T A, Boos W R. 2012. The tropospheric response to tropical and subtropical zonally asymmetric torques: Analytical and idealized numerical model results. J Atmos Sci, 69: 214–235

Shepherd T G. 2014. Atmospheric circulation as a source of uncertainty in climate change projections. Nat Geosci, 7: 703–708

Sigmond M, Shepherd T G. 2014. Compensation between resolved wave driving and parameterized orographic gravity wave driving of the Brewer-Dobson circulation and its response to climate change. J Clim, 27: 5601–5610

Teixeira M A C, Argain J L. 2022. The drag exerted by weakly dissipative trapped lee waves on the atmosphere: application to Scorer's two layer model. Q J R Meteorol Soc, 148: 3183–3202

Tian S F, Yasunari T. 1998. Climatological aspects and mechanism of spring persistent rains over Central China. J Meteorol Soc Japan, 76: 57–71

van Niekerk A, Sandu I, Vosper S. 2018. The circulation response to resolved versus parametrized orographic drag over complex mountain terrains. J Adv Model Earth Syst, 10: 2527–2547

Wan R, Wu G. 2007. Mechanism of the spring persistent rains over southeastern China. Sci

China Ser D-Earth Sci, 50: 130–144

Wang F, Yang S, Wu T. 2014. Radiation budget biases in AMIP5 models over the East Asian monsoon region. J Geophys Res, 119: 13400–13426

Wu G, Duan A, Liu Y, Mao J, Ren R, Bao Q, He B, Liu B, Hu W. 2015. Tibetan Plateau climate dynamics: recent research progress and outlook. Nat Sci Rev, 2: 100–116

Wu G, Liu Y, He B, Bao Q, Duan A, Jin F F. 2012. Thermal controls on the Asian summer monsoon. Sci Rep, 2: 404

Wu G, Liu Y, Wang T, Wan R, Liu X, Li W, Wang Z, Zhang Q, Duan A, Liang X. 2007. The influence of mechanical and thermal forcing by the Tibetan Plateau on Asian climate. J Hydrometeorol, 8: 770–789

Xu X, Li R, Teixeira M A C, Lu Y. 2021. On the momentum flux of vertically propagating orographic gravity waves excited in nonhydrostatic flow over three-dimensional orography. J Atmos Sci, 78: 1807–1822

Xu X, Song J, Wang Y, Xue M. 2017. Quantifying the effect of horizontal propagation of three-dimensional mountain waves on the wave momentum flux using Gaussian beam approximation. J Atmos Sci, 74: 1783–1798

Xu X, Zhao T, Lu C, Guo Y, Chen B, Liu R, Li Y, Shi X. 2014. An important mechanism sustaining the atmospheric "water tower" over the Tibetan Plateau. Atmos Chem Phys, 14: 11287–11295

Yeh T C. 1950. The circulation of high troposphere over China in winter of 1945–46. Tellus, 2: 173–183

Zhang L, Zhou T, Chen X, Wu P, Christidis N, Lott F C. 2020. The late spring drought of 2018 in South China. Bull Am Meteorol Soc, 101: S59–S64

Zhang R, Xu X, Wang Y. 2020. Impacts of different orographic drag on the summer monsoon circulation and precipitation in East Asia. J Geophys Res, 125: e2019JD032337

Zhang Y, Chen H, Yu R. 2014. Simulations of stratus clouds over Eastern China in CAM5: Sensitivity to horizontal resolution. J Clim, 27: 7033–7052

Zhao P, Zhang R, Liu J, Zhou X, He J. 2007. Onset of southwesterly wind over eastern China and associated atmospheric circulation and rainfall. Clim Dyn, 28: 797–811

Zhou X, Beljaars A, Wang Y, Huang B, Lin C, Chen Y, Wu H. 2017. Evaluation of WRF

simulations with different selections of subgrid orographic drag over the Tibetan Plateau. J Geophys Res, 122: 9759–9772

Zhou X, Yang K, Beljaars A, Li H, Lin C, Huang B, Wang Y. 2019. Dynamical impact of parameterized turbulent orographic form drag on the simulation of winter precipitation over the western Tibetan Plateau. Clim Dyn, 53: 707–720